Formation of Multi-Compartment Condensates through Aging of Protein-RNA Condensates

Katarzyna Makasewicz, Timo N. Schneider, Prerit Mathur, Stavros Stavrakis, Andrew J. deMello, and Paolo Arosio*

Department of Chemistry and Applied Biosciences ETH Zurich, Vladimir Prelog Weg 1, 8093, Zurich, Switzerland

E-mail: katarzyna.makasewicz@chem.ethz.ch,paolo.arosio@chem.ethz.ch

Abstract

Cells can dynamically organize reactions through the formation of biomolecular condensates. These viscoelastic networks exhibit complex material properties and mesoscale architectures, including the ability to form multi-phase assemblies. Understanding the molecular mechanisms underlying the formation of compartmentalized condensates has implications not only in biology but also in the development of advanced materials. In this study, we demonstrate that the aging of heterotypic protein-RNA condensates can lead to the formation of double-emulsion structures. By combining fluorescence-based techniques with theoretical modeling, we show that, as the condensates age, the strengthening of homotypic protein-protein interactions induces the release of RNA molecules from the dense phase. Notably, when condensates exceed a critical size, the slow diffusion of RNA molecules triggers the nucleation of a dilute phase within the protein-rich condensates, ultimately resulting in the formation of double-emulsion structures. These findings illustrate a new mechanism for a formation of dynamic multi-compartment condensates.

Introduction

Increasing evidence suggests that cells can orchestrate reactions in space and time by forming membraneless organelles known as biomolecular condensates.[1–4] These condensates are viscoelastic networks that can exhibit complex structure and material properties.[5,6] In many cases, multi-component condensates can give rise to multi-phase assemblies.[7–9] One notable example is the nucleolus, a membraneless organelle consisting of sub-compartments having distinct material properties.[10,11] This multilayered structure plays a crucial role in coordinating the spatial and temporal biochemical events involved in ribosome biogenesis. The N- and C-terminal domains of TDP-43, a ribonucleoprotein associated with stress granules, have also been observed to form multi-phase condensates within the cell.[12] In a ribonucleoprotein/polyU system, double emulsions are observed at high RNA-protein ratios, which can be attributed to reentrant phase behaviour.[13–15] In mixtures containing different proteins and RNA molecules, multiphasic condensates can exhibit different morphologies as a function the relative strength of protein-protein and protein-RNA interactions, as well as protein-RNA stoichiometry.[16–20] Multi-compartment structures can also form during rapid temperature cycling, as seen with condensates consisting of polyA RNA and PEG,[21] where fast cooling leads to a change in equilibrium composition and, due to the slow diffusion of the macromolecules, nucleation of the dilute phase inside larger condensates.[21]

Many condensates exhibit non-equilibrium architectures and age over time, transitioning towards lower energy states.[5,22–25] In such a process, intermolecular forces among the components of the condensates exhibit gradual non-conservative changes, which may be linked to conformational changes of the macromolecules.

In this study, we demonstrate that the aging of heterotypic condensates can spontaneously lead to the formation of double-emulsion structures without changes in external variables such as temperature or solution conditions. We analyze heterotypic condensates composed of the DEAD-box protein Dhh1[26] and an RNA model, polyU, by applying a combination of fluorescence correlation spectroscopy (FCS), fluorescence lifetime imaging (FLIM) and

theoretical modeling. Both FLIM and FCS are time-resolved techniques that enable the investigation of local molecular environments, which are generally inaccessible to standard bright-field and fluorescence imaging methods. We show that, under the investigated conditions, the strength of homotypic protein-protein interactions increases over time, resulting in the release of polyU molecules from the dense phase. For condensates above a critical size, low diffusivity and long diffusion paths lead to nucleation of a dilute phase inside the condensates. These findings provide insights into a mechanism for the formation of multi-compartment condensates. The implications have significance in the material sciences for the development of kinetically arrested double emulsions based on sub-structured condensates. These could potentially lead e.g. to microcapsules, with applications in protein release.[27]

Results and discussion

Condensates of Dhh1-mCh with and without polyU age over time

We first employed bright-field microscopy to investigate the morphological changes of condensates composed of 20 μM mCherry-tagged Dhh1 (Dhh1-mCh) on the timescale of several days. Phase separation was induced by diluting the stock solution at high salt (200 mM NaCl) in 18 mM HEPES-KOH 90 mM KCl 1.2 mM $MgCl_2$ buffer at pH 6.0. Samples were incubated for 1 h before imaging. Figure 1A shows bright-field images of Dhh1-mCh droplets collected at different time points after inducing phase separation. Initially, all droplets showed spherical morphology and relatively rapid fusion events (within seconds) indicative of their liquid-like character. After 24 h, the droplets developed non-spherical morphologies with no further fusion events being observed. Property changes of the Dhh1-mCh condensates over time was further confirmed using fluorescence recovery after photobleaching (FRAP), which showed a 50% decrease in recovery after 48 h compared to freshly prepared droplets (imaged within 2 h after preparation) (Figure S1A).

Next, we followed the aging of Dhh1-mCh condensates formed in the presence of 0.1 mg/ml

polyU with a degree of polymerization of 20 (polyU-20) (Figure 1B). As in the case of homotypic Dhh1-mCh condensates, the heterotypic Dhh1-mCh-polyU-20 condensates initially display spherical morphology and fuse rapidly (within seconds). Interestingly, upon incubation, the condensates developed a double emulsion structure within 24 h. Within 48 h, the entrapped droplets underwent coalescence, which resulted in the formation of a core-shell structure. Importantly, only large droplets with diameters above 25 μm developed the double-emulsion/core-shell morphology. In contrast, smaller droplets remained spherical and did not show any signs of double emulsion formation. Similarly to homotypic Dhh1-mCh condensates, FRAP experiments showed a 50% decrease in protein fluorescence recovery in droplets imaged 48 h after preparation as opposed to droplets imaged 2 h after preparation. (Figure S1B).

We also followed the morphological changes of the Dhh1-mCh condensates with longer RNA mimics, polyU-50 (Figure 1C) and polyU-3000 (Figure 1D). In the case of droplets with polyU-50, we observed similar morphological changes as in the case of droplets with polyU-20 but on a longer timescale (72 hours as compared to 48 h for droplets with polyU-20). For the Dhh1-mCh droplets with polyU-3000, no morphological changes were observed over the timescale of the experiment (up to 8 days).

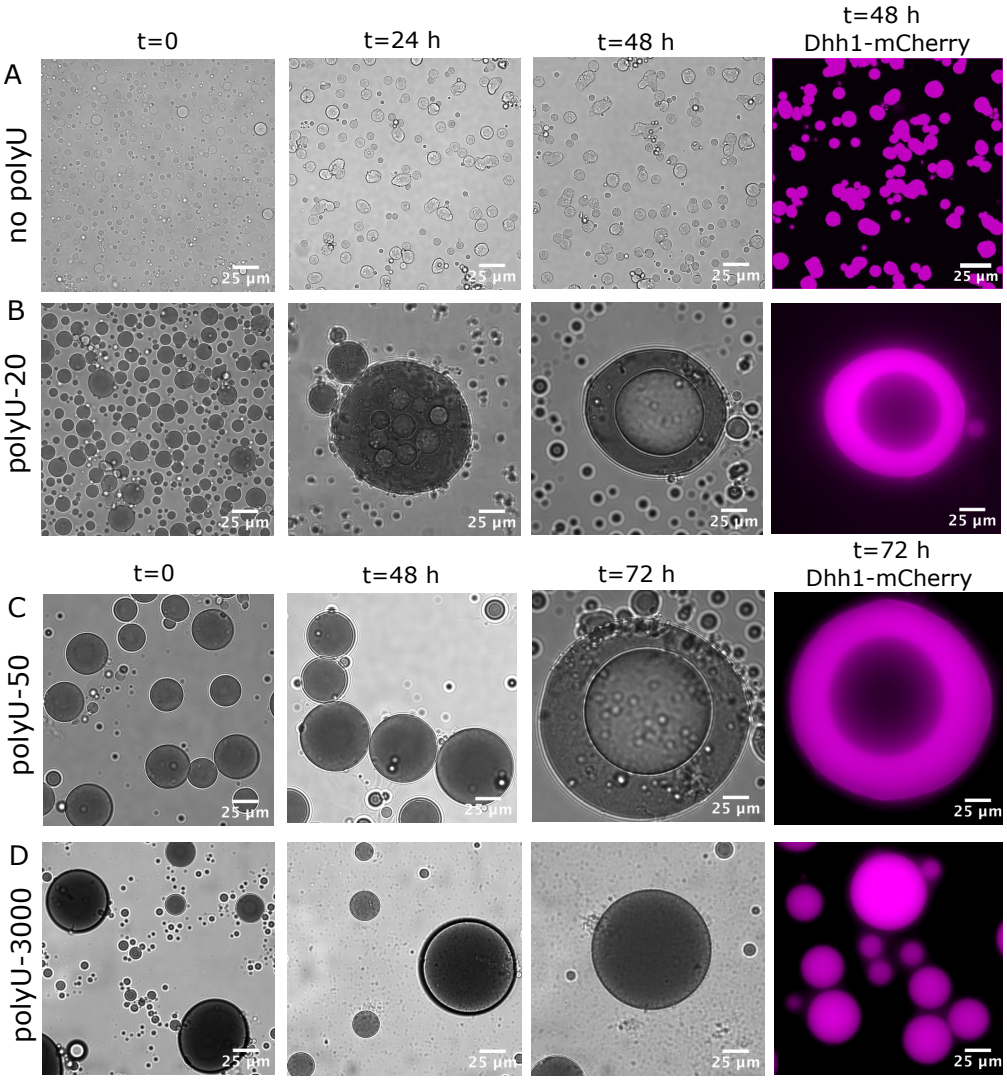

Figure 1: Aging of Dhh1-mCh condensates with and without polyU of different lengths. Brightfield and fluorescence microscopy images collected at different time points for Dhh1-mCh samples in the absence (A) and presence of 0.1 mg/ml polyU-20 (B), 0.1 mg/ml polyU-50 (C) and 0.1 mg/ml polyU-3000 (D).

Probing the concentration of polyU-20 in the dilute phase using FCS

We next investigated how condensate aging affects the partitioning of polyU in the dilute and dense phases. To do this, we measured polyU concentration in the dilute phase by fluorescence correlation spectroscopy (FCS). We prepared condensates of 20 μM Dhh1-mCh and 0.1 mg/mL polyU-20 (corresponding to 15 μM) including 1% polyU-20 labelled at

the 3′ end with carboxyfluorescein (polyU-FAM). The FCS auto-correlation curve contains information regarding both the diffusion coefficient and the concentration of fluorescently labelled molecules. We acquired FCS data on fresh samples (up to 2 h after inducing phase separation) and after 48 h (Figure 2A). The auto-correlation curves at both time points were fitted to a model that assumes the presence of a single diffusing component, yielding a D_{coeff} = 147 ± 4 μm^2/s (mean ± standard deviation, n=4), which is equal to the value measured in a homogeneous dilute solution of monomeric polyU-FAM (D_{coeff} = 151 ± 5 μm^2/s, n=4). Based on the amplitude of the auto-correlation curve, the total polyU concentration in the dilute phase of fresh samples was calculated to be equal to 2.1 ± 0.2 μM (mean ± SD, n=4). Here, we assume that labelled and unlabelled polyU partition equally between the dilute and dense phases. The decrease in the amplitude of the auto-correlation curve over time indicates an increase in the polyU concentration in the dilute phase, which after 48 h was 3.6 ± 0.4 μM (mean ± SD, n=4).

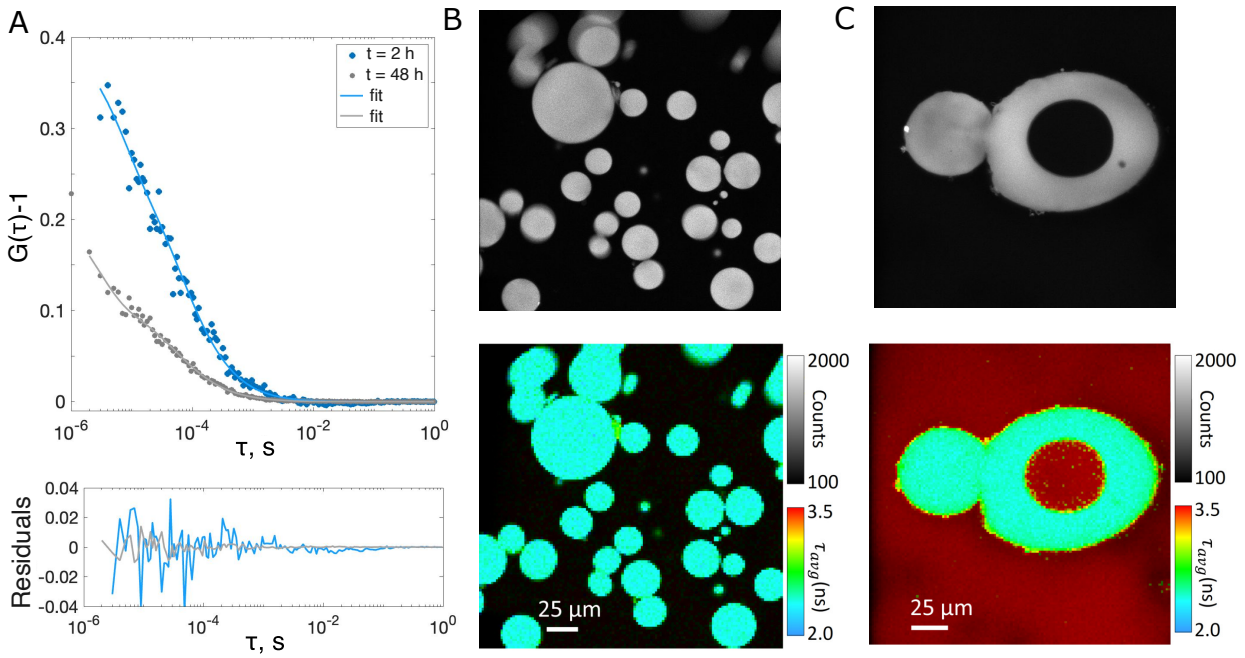

Figure 2: Migration of polyU from the dense phase into the dilute phase upon condensate aging. A) Fluorescence correlation spectroscopy: auto-correlation curves acquired on FAM-labelled polyU-20 in the dilute phase coexisting with Dhh1-mCh-polyU-FAM condensates in a fresh sample (t = 2 h) and after 48 h. The correlation curves were fitted to a model assuming a single diffusing component with a triplet contribution. Fitting residuals are displayed below the figure. Both fits yielded a diffusivity of 147 ± 4 $\mu m^2/s$. The decrease in the auto-correlation amplitude over time indicates that the polyU concentration in the dilute phase increases over time. The total polyU concentration in the dilute phase was 2.1 ± 0.2 μM after 2 h and 3.6 ± 0.4 μM after 48 h. B and C) Fluorescence intensity (top) and fluorescence lifetime (FLIM) images (bottom) of Dhh1-mCh-polyU-20 condensates with 1% polyU-FAM after 2 h (B) and after 48 h (C).

Probing Dhh1-polyU interactions with FLIM

The results described in the preceding sections suggest that, over time, the strength of protein-protein interactions increases (as shown by aging of Dhh1-mCh condensates without polyU), with a fraction of polyU molecules being released into the dilute phase. To further investigate the protein-polyU interactions, we performed fluorescence lifetime imaging microscopy (FLIM) on the same samples as those analysed by FCS by monitoring the fluorescence lifetime of carboxyfluorescein conjugated to polyU-20. The fluorescence lifetime of monomeric polyU-FAM at low concentrations in the buffer used in our experiments (10

mM TRIS pH 6.0) was measured to be 3.65 ± 0.02 ns (Figure S2). When recruited into Dhh1-mCh condensates, the lifetime of poly-FAM decreased to 2.3 ± 0.1 ns (Figure 2B). In fresh Dhh1-mCh-polyU condensates, the polyU-FAM concentration in the dilute phase is too low to yield meaningful FLIM data, and therefore the lifetime histogram reconstructed for fresh condensates displays a single peak centered at approximately 2 ns, corresponding to the polyU-FAM within the condensates (Figure S3). However, after 48 h, a population characterized by a fluorescence lifetime centered around 3.6 ns emerges (Figure S3). This second peak is consistent with the FLIM image shown in Figure 2C, demonstrating that, after 48 h, polyU-FAM (with a longer lifetime) is present both outside the condensate and within the core of the condensate. The average lifetime within the condensates is 2.2 ± 0.01 ns. Interestingly, a shell characterized by an intermediate average lifetime of 2.63 ± 0.17 ns appears on the surface of the condensates.

The observed changes in the fluorescence lifetime of polyU-FAM in the dilute and dense phase could be due to many factors, including changes in the refractive index, viscosity, or pH between the two phases. The fluorescence lifetime of FAM was previously shown to be independent of the viscosity of the medium.[28] The pH effect can also be excluded, since the lifetime of fluorescein was reported to increase from 3.6 ± 0.1 ns at pH 3 to 5.0 ± 0.4 ns at pH 10.[29] We also performed control experiments that excluded also the effect of the refractive index (see Supplementary Information and Figure S4).

Other factors affecting the fluorescence lifetime inside the condensates are fluorescence quenching and Förster resonance energy transfer (FRET)[30] between polyU-FAM and Dhh1-mCh. The latter could occur with the carboxyfluorescein acting as a donor and the mCherry as an acceptor. FRET would result in the decrease of the lifetime of the donor, because the fluorophores, which reside longer in the excited state, have higher probability of participating in the energy transfer.[30] The occurrence of FRET would suggest a strong interaction between Dhh1-mCh and polyU-FAM within the condensates. Fluorescence quenching inside

the condensate may occur due to the high fluorophore concentration. In order to check this effect, we added FITC into a sample of phase separated Dhh1-mCh condensates with fully unlabelled polyU-20. Similarly to the case when the fluorophore is conjugated to polyU, we also observed a drop in fluorescence lifetime to 2.26 ± 0.01 ns (Figure S5). Accordingly, fluorescence quenching is likely responsible for the decrease in lifetime of polyU-FAM upon partitioning into the condensates.

Overall, our analysis indicates that the decrease of polyU-FAM lifetime upon incorporation into the Dhh1-mCh condensates may be due to FRET, fluorescence quenching or a combination of these effects. Independently of the exact mechanism, FLIM data demonstrate that, as the condensates age, polyU diffuses from the dense phase into the dilute phase, which is consistent with the FCS results. This suggests that condensate aging involves a decrease in the strength of the net Dhh1-mCh-polyU interactions, which is in agreement with the increase of protein-protein interactions shown by aging of homotypic Dhh1-mCh condensates (Figure 1A and S1A).

Decrease of net Dhh1-polyU interactions upon aging

In order to further confirm the decrease of the net Dhh1-mCh-polyU interaction strength over time, we designed an experiment in which we prepared homotypic condensates of Dhh1-mCh and added polyU-FAM after incubating the samples for 1 h or 24 h. As shown in Figure 3A, when polyU-FAM was added to homotypic Dhh1-mCh condensates incubated for 1 h, within 20 min most of the droplets in the sample became homogeneously fluorescent in the FAM channel, indicating that polyU-FAM partitioned into and diffused within condensates until reaching an equilibrium dense phase concentration. In addition to the recruitment of polyU into existing Dhh1-mCh condensates, the introduction of polyU promoted the formation of new condensates containing both Dhh1-mCh and polyU-FAM due to the decrease of the saturation concentration required for phase separation, driven by the additional contribution of attractive heterotypic interactions to homotypic protein-protein interactions.

The fluorescence intensity within the condensates was homogeneous and similar among the different droplets, implying a uniform polyU-FAM concentration in the condensate population. The diffusion of polyU-FAM within the condensates occurred over a period of 20 minutes. Considering a typical diffusion distance inside the condensates of 3.5 μm, this timescale corresponds to a diffusion coefficient on the order of 0.01 $\mu m^2/s$, i.e. $1.5 \cdot 10^3$ fold lower than the diffusivity in the dilute phase. Such a low diffusivity is ascribed to high concentrations and strong interactions between the macromolecules inside the condensates.

In analogy to fresh Dhh1-mCh condensates, the addition of polyU-FAM to Dhh1-mCh samples incubated for 24 h led to the formation of new condensates (Figure 3B). However, the partitioning and diffusion of polyU within aged droplets proceeded over a longer timescale. Indeed, after 30 minutes, the fluorescence intensity of polyU-FAM in the center of aged droplets remained relatively low. From this timescale and the typical diffusion distance from the rim to the center of the droplets (3 μm), we estimated the upper bound of the polyU diffusivity in the aged droplets to be approximately 0.001 $\mu m^2/s$.

Importantly, the protein condensates incubated for 1 h and 24 h displayed significantly different fluorescence intensities after polyU addition, with higher fluorescence intensity of FAM observed in fresh condensates, implying higher polyU concentrations compared to aged droplets. Thus, these data show that the equilibrium concentration of polyU in the aged condensates is lower than in the fresh condensates, confirming the reduced protein-polyU interaction strength as a result of the strengthening of protein-protein interactions during aging.

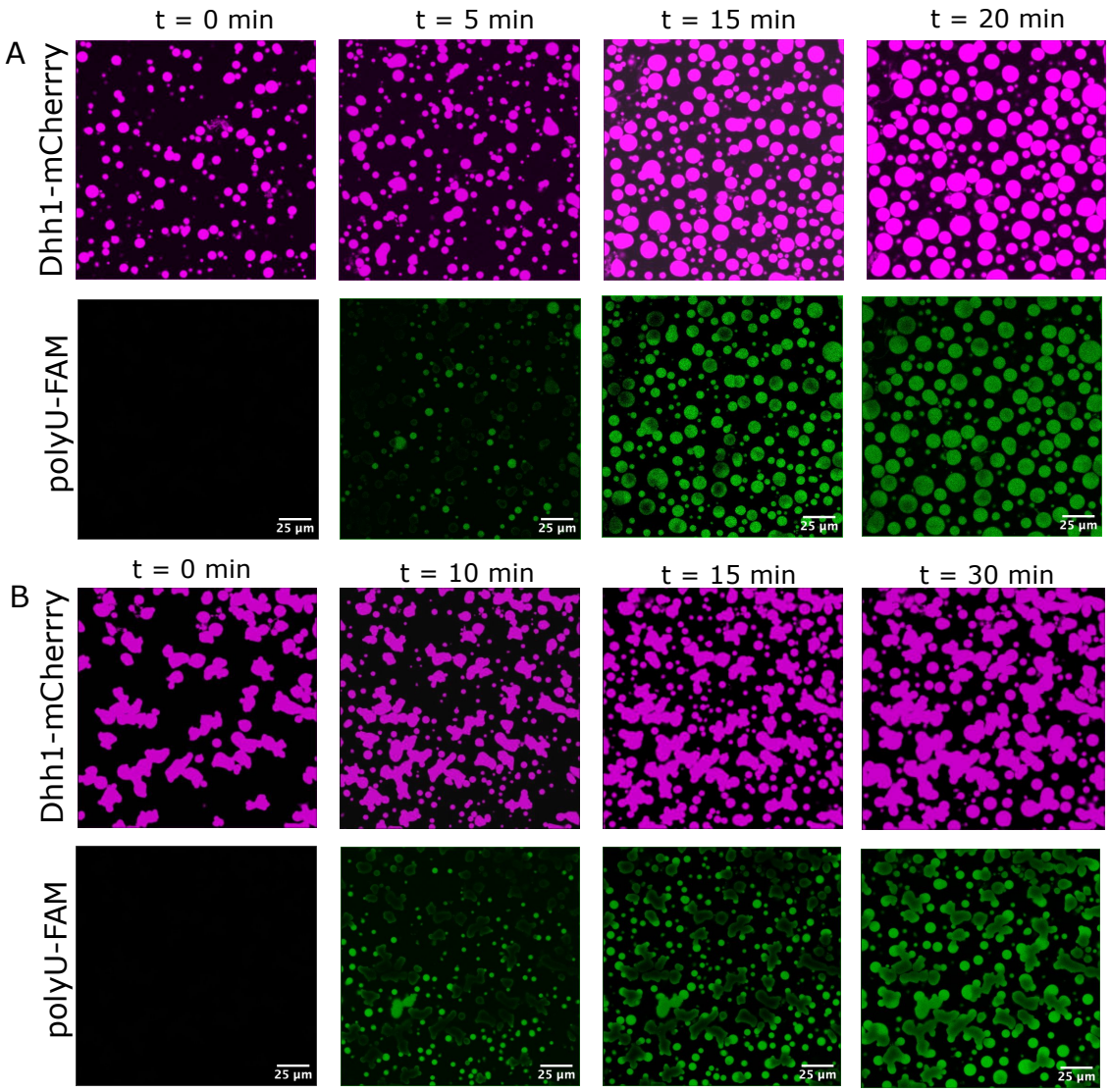

Figure 3: Partitioning of polyU-FAM into fresh and aged Dhh1-mCh condensates. A) PolyU-FAM was added to Dhh1-mCh condensates incubated for 1 h after inducing phase separation. B) PolyU-FAM was added to Dhh1-mCh condensates incubated for 24 h. The samples were monitored over time to track the recruitment of polyU into existing droplets and the appearance of new (spherical) condensates due to the decrease of the saturation concentration for phase separation in the presence of polyU.

Cahn-Hilliard theory describes the formation of double-emulsion condensates

The experimentally observed nucleation of a dilute phase (Figure 1B,C and Figure 2C) within the Dhh1-mCh-polyU condensates can be explained by a decrease in the relative strength

of protein-polyU interactions with time combined with the slow diffusion of polyU and protein inside the dense phase. The observed size-dependent morphology further supports this mechanism, as nucleation of the dilute phase is observed only in large condensates, suggesting a kinetic rather than a thermodynamic effect. Large droplets exhibit a slower response to changes in equilibrium compositions due to longer diffusion paths, which can lead to meta-stable or unstable compositions. Our experimental results can be quantitatively rationalized using the Cahn-Hilliard phase field model.[31] The governing equation that describes the evolution of the order parameter ϕ in time and space is given by:[32]

$$\frac{\partial \phi}{\partial t} = \nabla \cdot M(\phi) \nabla \mu \tag{1}$$

where

$$\mu = \frac{\partial F}{\partial \phi} - \epsilon^2 \Delta \phi \quad . \tag{2}$$

Here, μ represents the chemical potential, $M(\phi)$ the composition-dependent mobility, and t the time. The chemical potential μ consists of a bulk term (related to the free energy of the system F, first term on right hand side of Equation 2) as well as a surface term (second term on right hand side of Equation 2), where the parameter ϵ is related to the surface tension. At equilibrium, the chemical potential must be identical everywhere, resulting in all time derivatives being zero.

Applying this model to a ternary mixture of protein, polyU and solvent, we obtain coupled partial differential equations (1) with the volume fractions of protein (ϕ_p) and polyU (ϕ_u) as order parameters. The free energy of the system F, according to the Flory-Huggins model, is given by:[33]

$$F(\phi_p, \phi_u) = \frac{\phi_p}{N_p} \ln(\phi_p) + \frac{\phi_u}{N_u} \ln(\phi_u) + \frac{\phi_s}{N_s} \ln(\phi_s) + \chi_{pu} \phi_p \phi_u + \chi_{ps} \phi_p \phi_s + \chi_{us} \phi_u \phi_s \tag{3}$$

Here, the solvent volume fraction is given by $\phi_s = 1 - \phi_p - \phi_u$, χ_{pu}, χ_{ps} and χ_{us} are binary interaction coefficients for protein-polyU, protein-solvent and polyU-solvent, while N_p, N_u and N_s are the number of monomers for protein/polyU and 1 for the solvent. Under the experimental conditions used in this work, Dhh1-mCh undergoes phase separation in the absence of polyU (Figure 1A), indicating that the interaction parameter χ_{ps} is positive. We chose negative values for χ_{pu} and χ_{us} that lead to phase separation in a range of polyU and protein concentrations consistent with experimental data. All model parameters are shown in Table S1, and additional details concerning their choice are reported in Materials and Methods.

The starting point of all simulations is a droplet rich in protein and polyU at equilibrium with the dilute phase. The concentrations in the dilute and dense phase were calculated based on the interaction parameters defined above and the total concentrations of protein and polyU used in the experiments. In order to model aging, we linearly increased the strength of homotypic protein-protein interactions over time, leading to a simultaneous increase of the parameters χ_{pu} and χ_{ps}. We note that a decrease in the protein-polyU interaction strength may also occur in the system. However, we preferred to keep a minimalistic version of the model and expect that similar trends would be observed with contributions from decreased protein-polyU interactions.

Figure 4A shows the simulation of a 30 μm condensate obtained from a solution with 20 μM Dhh1-mCh and 0.1 mg/mL polyU-20 (same conditions of the experiments shown in Figure 1B). The increasing strength of protein-protein interaction over time leads to droplet shrinking and an increase of protein concentration in the dense phase. Droplet shrinking initially increases the concentration of polyU in the dense phase, which later decreases due to the decrease of the net protein-polyU interactions. The release of polyU from the dense phase is consistent with the increase in concentration of polyU in the dilute phase measured by FCS (Figure 2A). Although the Cahn-Hilliard model does not provide a good description of interfacial properties, it is interesting to note that the modelling predicts maximum polyU

concentrations at the interface. This may result from the balance of interactions in the aged system, with protein-polyU interactions being stronger than protein-solvent interactions, and polyU-solvent and polyU-protein interactions being of comparable strength. This non-trivial behaviour is consistent with the results obtained by FLIM on aged droplets, which show a rim of FAM lifetime intermediate between the lifetime inside and outside of the condensates (Figure 2C).

We next applied the model to rationalize the effect of droplet size on the observed formation of double-emulsion condensates over time. Simulations with the 30 μm diameter droplet showed that the properties of the condensates changed over time but no double-emulsion was formed. In contrast, simulations of a droplet with a larger initial diameter (60 μm) indicated that the longer diffusion paths for macromolecules led to nucleation of a dilute phase inside the dense phase (Figure 4B). This is consistent with the experimental observation that double-emulsions were formed only in condensates exceeding a critical size (approx. 20 μm in diameter).

To probe the effect of polyU length, we performed the same simulations with polyU-50 and observed an increase in the threshold droplet diameter and of the time required to form double emulsions (Figure S6). The larger critical droplet diameter observed with polyU-50 may seem counter-intuitive, since the 2.5 fold slower diffusion of polyU-50 compared to polyU-20 is expected to facilitate nucleation of a dilute phase inside the dense phase. However, due to the larger molecular size and thus greater number of protein interactions sites per polyU molecule, polyU-50 displays overall stronger interaction with the protein and therefore a lower tendency to migrate towards the dilute phase.

All together, the model is capable of rationalizing the observed experimental trends for protein-polyU-20 and protein-polyU-50 condensates, further confirming the proposed mechanism underlying the formation of substructures upon aging.

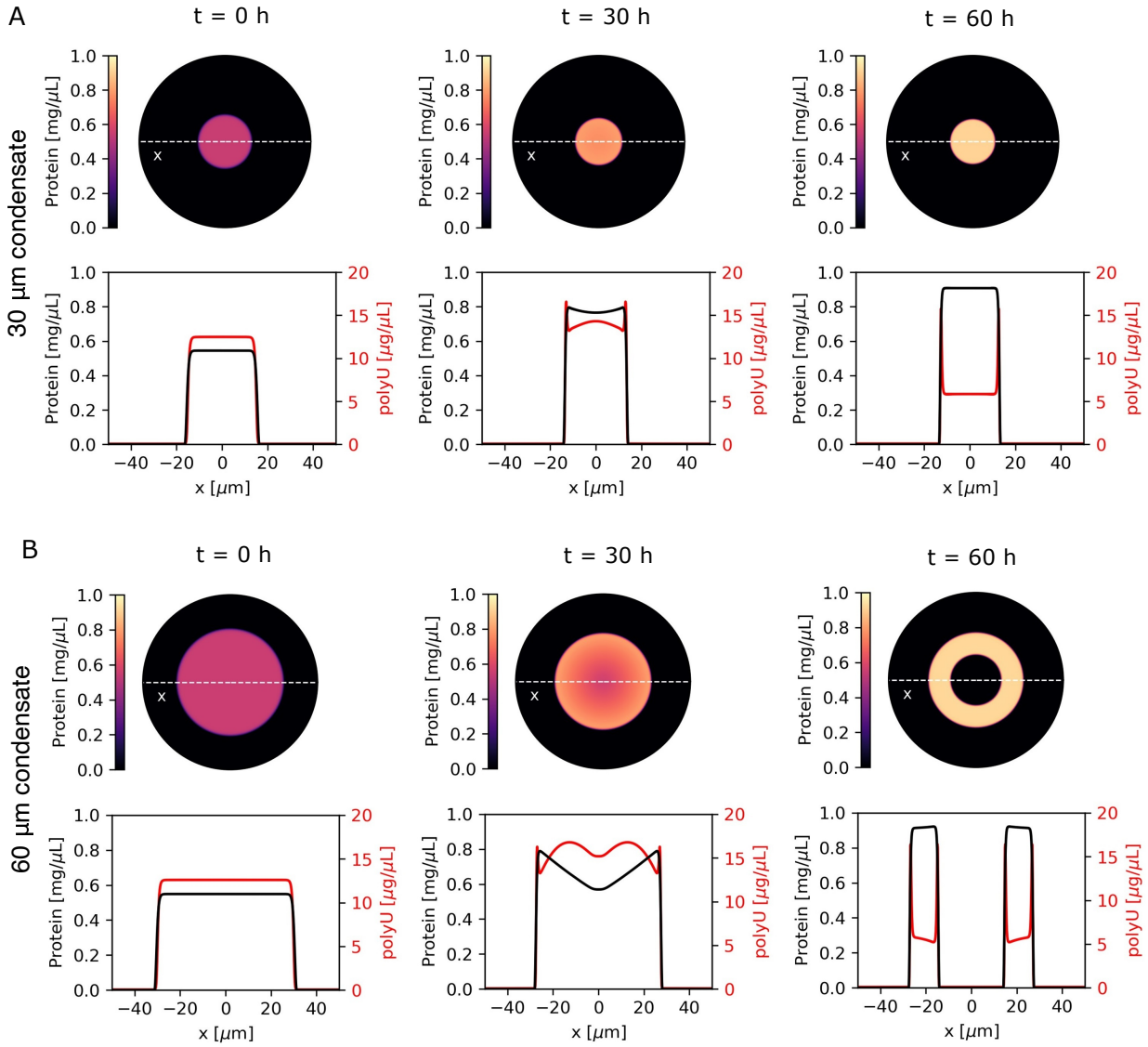

Figure 4: Simulations of aging of Dhh1-polyU condensates based on the Cahn-Hilliard model, showing how the changes in interaction strength combined with the slow polyU diffusion leads to size-dependent morphology of the aged condensates. Simulation results for condensates with polyU-20 and initial condensate size of 30 μm (A) and 60 μm (B). For 60 μm initial diameter, a dilute phase nucleates inside the condensate, while for 30 μm, the condensate shrinks and polyU migrates to the dilute phase.

Conclusions

We have shown that heterotypic Dhh1-mCh-polyU condensates undergo aging over time, which results in the formation of multi-compartment architectures depending on the con-

densate size. By a combination of experimental and computational approaches, we have demonstrated that a net decrease in the strength of protein-polyU interactions triggers the release of polyU molecules into the dilute phase. For condensates smaller than a critical size, the diffusion of polyU from the dense to the dilute phase leads to shrinking of the condensate without a change in morphology. For condensates larger than a critical size, a dilute phase nucleates inside the dense phase, leading to the formation of a double-emulsion structure. This process is ascribed to the slow diffusion inside the dense phase, which constitutes a limiting step to attaining the new equilibrium concentrations in the dense and dilute phases as the aging proceeds. This work shows that multi-compartment architectures can originate in non-equilibrium condensates undergoing aging over time, leading to kinetically-arrested double emulsion.

Materials and Methods

Protein purification

Recombinant Dhh1 with an N-terminal 6xHis tag and C-terminal mCherry tag were expressed in E. coli BL21 DE3 cells as described previously.[34] The protein was first purified by affinity chromatography using Ni^{2+} charged Fast Flow Chelating Sepharose matrix (Cytiva Sweden AB, Uppsala, Sweden) and by size exclusion with a HiLoad 16/600 Superdex 200 pg column (Cytiva Sweden AB, Uppsala, Sweden). The elution buffer at pH 7.5 contained 300 mM NaCl, 25 mM Tris, 2 mM 2-Mercaptoethanol, and 10% glycerol. Selected fractions from size exlusion chromatography were concentrated to approx. 400 μM using Amicon 10 000 MWCO spin filters and flash-frozen in liquid N_2 in 5-10 μl aliquots.

polyU

Lyophilized polyuridilic acid (polyU) containing 20 and 50 nucleotides (polyU-20 and polyU-50) and polyU-20 labelled at 3′ end with carboxyfluorescein (FAM) were purchased from

Microsynth AG (Baglach, Switzerland). High molecular weight polyU (average degree of polymerization of 2860) was purchased from Sigma Aldrich, Buchs, Switzerland.

Sample preparation and imaging

Droplet formation was induced by dissolving the protein stock solution in a low salt buffer (18 mM HEPES, 90 mM KCl, 1.2 mM $MgCl_2$) in the presence or absence of 0.1 mg/ml polyU. All samples were prepared and analyzed in glass bottom 384-well plates (Brooks, Matriplate) at a final volume of 20 μl. In order to prevent evaporation during long term incubation, the wells adjacent to the ones containing the samples were filled with 150 mM NaCl solution and the plate was closed with aluminum tape. Samples were imaged by widefield microscopy performed on an inverted epi-fluorescence microscope (Nikon Eclipse Ti-E; MicroManager software, version 2.0-gamma) equipped with a Plan Apo 60x 1.4 NA oil immersion objective (Nikon), an LED light source (Omicron LedHUB Light engine; Omicron Software, version 3.9.28) and an Andor Zyla sCMOS camera.

Fluorescence recovery after photobleaching

FRAP experiments were performed on a Nikon Spinning Disk SoRa confocal microscope equipped with sCMOS Hamamtasu Orca Fusion BT camera. 100x 1.45 CFI Plan Apo oil immersion objective was used. Samples were bleached and imaged using a 561 nm laser. For each experiment, a region of interest (ROI) within a protein condensate with size of approx. 10% of its diameter was chosen. For each measurement an ROI of the same size was placed in another condensate for background correction. Fluorescence recovery was measured over 120 s post bleaching. Data were analyzed using Nikon NIS Elements software. Data presented in Figure S1 represent the background-corrected and normalized mean and standard deviation of fluorescence intensities acquired for 3 different condensates for each sample and time point.

Fluorescence correlation spectroscopy

FCS experiments were performed on an inverted confocal fluorescence microscope (Leica SP8 STED, Leica Application Suite X (LAS X) software, version 1.0) equipped with a HC PL APO CS2 63x 1.2 NA water immersion objective with a software-controlled correction collar (Leica) and a hybrid detector for single molecule detection (HyD SMD). The confocal volume was calibrated using Atto 488 NHS Ester (D_{coeff} = 400 μm^2/s), which yielded an effective volume, V_{eff}, of 0.6 ± 0.1 fl and a focal volume height-width ratio, $\kappa = 9$. The samples were excited with a 488 nm laser (from a white Light Laser at 80 MHz) and the fluorescence emission collected between 500 and 530 nm.

Fluorescence lifetime imaging microscopy

FLIM experiments were performed on an inverted confocal fluorescence microscope (Leica SP8 STED, Leica Application Suite X (LAS X) software, version 1.0) equipped with a HC PL APO CS2 63x 1.2 NA water immersion objective with a software-controlled correction collar (Leica) and a hybrid detector for single molecule detection (HyD SMD). FLIM images of the droplets with polyU-FAM were acquired until 1000 photons per pixel were collected in the brightest channel. The samples were excited with a 488 nm laser (from a White Light Laser at 20 MHz) and the fluorescence emission collected between 500 and 530 nm. Data analysis was performed using SymPhoTime 64 2.1 software (PicoQuant, Berlin, Germany). Images were fitted pixel by pixel with a one component reconvolution model. The images and data shown in the text display the intensity and the intensity-weighted average fluorescence lifetime.

Cahn-Hilliard model

For the initial droplet in equilibrium with the dilute phase, the composition of dilute and dense phase as well as their volume fractions were calculated by minimizing the free energy

of the system f_{sep} as described by Lin et al.[35]

$$f_{sep} = \nu f(\phi_p^\alpha, \phi_u^\alpha) + (1-\nu) f(\phi_p^\beta, \phi_u^\beta) \tag{4}$$

with f being defined in equation (3) and ν the volume fraction of dense phase. We considered the total concentrations of 20 μM Dhh1-mCh and 0.1 mg/mL polyU used in experiments, and protein and polyU densities of 1.35 g/mL[36] and 1.5 g/mL,[37] respectively. N_p, N_u and N_s in the Flory-Huggins free energy model (Eq. 3) were set equal to the number of residues (protein: 748, polyU: 20/50, solvent: 1).

The values of the binary interaction coefficients were set to χ_{pu}: -2, χ_{ps}: 0.7 and χ_{us}: -0.7 to simulate phase separation in a range of polyU and protein concentrations consistent with experimental data. The change in the strength of protein-protein interactions during aging process was modelled by a linear increase of the value of χ_{pu} from -2 to -1.7 and of χ_{ps} from 0.7 to 1, over 48 h.

Following a common assumption,[32] the same interfacial parameter ϵ was considered for protein and polyU:[31]

$$\epsilon^2 = \left(\frac{l}{\Delta\phi}\right)^2 \Delta f_{max} \ , \tag{5}$$

where Δf_{max} is the maximum free energy difference between the separated and mixed system, and $\Delta\phi$ is the difference in protein volume fraction (we considered only protein since it is the main component of the droplet). The length scale l, which represents the interface width, was assumed constant across simulations and equal to 2 μm.

In addition to the thermodynamic parameters that determine the chemical potential, the Cahn-Hilliard model (1) requires the definition of the mobility $M(\phi)$. As a first step, the initial diffusivity of polyU-20 within the dense phase was set to 0.05 $\mu m^2/s$, consistent with experimental estimates obtained by adding polyU to fresh Dhh1-mCh condensates (Figure 3A). This diffusivity can change during aging due to changes in concentrations within the condensates. As condensates are viscoelastic networks, it is difficult to model the viscosity of

the dense phase. Furthermore, polyU molecules are smaller than Dhh1 and may experience microviscosity rather than macroviscosity. As a fist approximation, we considered a linear dependence of viscosity on protein volume fraction ϕ_p. The diffusivity is expressed as:

$$D_i = \frac{D_{i,0}}{1 + k \cdot \phi_p} \tag{6}$$

Assuming a hydrodynamic radius of 1.5 nm for polyU-20 and 8 nm for Dhh1-mCh, initial diffusivity of protein in the dense phase is 0.01 $\mu m^2/s$. We set $k = 20$ to reproduce the polyU-20 diffusion coefficient in the dense phase that was estimated experimentally. All model parameters are summarized in Table S1. The mobility can finally be computed using the following expression:[32]

$$M_i = \frac{D_i}{\partial^2 f_{ideal}/\partial \phi_i^2} \tag{7}$$

With this approach, the Cahn-Hilliard model is equivalent to Fick's second law in the absence of any interactions ($\chi_{ij} = 0$). Equation (1) was solved in spherical coordinates assuming radial symmetry with the droplet being centered at the origin. Details concerning the numerical solution are provided in the SI.

Acknowledgements

We kindly acknowledge the European Research Council through the Horizon 2020 research and innovation programme for financial support (grant agreement No. 101002094). We thank Dorothea Pinotsi from the Scientific Centre for Optical and Electron Microscopy at ETH Zurich (ScopeM) for help with setting up the FCS and FLIM experiments.

References

(1) Banani, S. F.; Lee, H. O.; Hyman, A. A.; Rosen, M. K. Biomolecular condensates: organizers of cellular biochemistry. *Nature reviews Molecular cell biology* **2017**, *18*,

285–298.

(2) Boeynaems, S.; Alberti, S.; Fawzi, N. L.; Mittag, T.; Polymenidou, M.; Rousseau, F.; Schymkowitz, J.; Shorter, J.; Wolozin, B.; Van Den Bosch, L., et al. Protein phase separation: a new phase in cell biology. *Trends in cell biology* **2018**, *28*, 420–435.

(3) Pappu, R. V.; Cohen, S. R.; Dar, F.; Farag, M.; Kar, M. Phase transitions of associative biomacromolecules. *Chemical Reviews* **2023**,

(4) Shin, Y.; Brangwynne, C. P. Liquid phase condensation in cell physiology and disease. *Science* **2017**, *357*, eaaf4382.

(5) Jawerth, L.; Fischer-Friedrich, E.; Saha, S.; Wang, J.; Franzmann, T.; Zhang, X.; Sachweh, J.; Ruer, M.; Ijavi, M.; Saha, S., et al. Protein condensates as aging Maxwell fluids. *Science* **2020**, *370*, 1317–1323.

(6) Alshareedah, I.; Moosa, M. M.; Pham, M.; Potoyan, D. A.; Banerjee, P. R. Programmable viscoelasticity in protein-RNA condensates with disordered sticker-spacer polypeptides. *Nature communications* **2021**, *12*, 6620.

(7) Fare, C. M.; Villani, A.; Drake, L. E.; Shorter, J. Higher-order organization of biomolecular condensates. *Open biology* **2021**, *11*, 210137.

(8) Mountain, G. A.; Keating, C. D. *Methods in enzymology*; Elsevier, 2021; Vol. 646; pp 115–142.

(9) Lu, T.; Spruijt, E. Multiphase complex coacervate droplets. *Journal of the American Chemical Society* **2020**, *142*, 2905–2914.

(10) Lafontaine, D. L.; Riback, J. A.; Bascetin, R.; Brangwynne, C. P. The nucleolus as a multiphase liquid condensate. *Nature reviews Molecular cell biology* **2021**, *22*, 165–182.

(11) Feric, M.; Vaidya, N.; Harmon, T. S.; Mitrea, D. M.; Zhu, L.; Richardson, T. M.; Kriwacki, R. W.; Pappu, R. V.; Brangwynne, C. P. Coexisting liquid phases underlie nucleolar subcompartments. *Cell* **2016**, *165*, 1686–1697.

(12) Schmidt, H. B.; Rohatgi, R. In Vivo Formation of Vacuolated Multi-phase Compartments Lacking Membranes. *Cell Reports* **2016**, *16*, 1228–1236.

(13) Banerjee, P. R.; Milin, A. N.; Moosa, M. M.; Onuchic, P. L.; Deniz, A. A. Reentrant Phase Transition Drives Dynamic Substructure Formation in Ribonucleoprotein Droplets. *Angew. Chem. Int. Ed.* **2017**, *56*, 11354 –11359.

(14) Maharana, S.; Wang, J.; Papadopoulos, D. K.; Richter, D.; Pozniakovsky, A.; Poser, I.; Bickle, M.; Rizk, S.; Guillén-Boixet, J.; Franzmann, T. M., et al. RNA buffers the phase separation behavior of prion-like RNA binding proteins. *Science* **2018**, *360*, 918–921.

(15) Henninger, J. E.; Oksuz, O.; Shrinivas, K.; Sagi, I.; LeRoy, G.; Zheng, M. M.; Andrews, J. O.; Zamudio, A. V.; Lazaris, C.; Hannett, N. M., et al. RNA-mediated feedback control of transcriptional condensates. *Cell* **2021**, *184*, 207–225.

(16) Kaur, T.; Raju, M.; Alshareedah, I.; Davis, R. B.; Potoyan, D. A.; Banerjee, P. R. Sequence-encoded and composition-dependent protein-RNA interactions control multiphasic condensate morphologies. *Nature communications* **2021**, *12*, 872.

(17) Chew, P. Y.; Joseph, J. A.; Collepardo-Guevara, R.; Reinhardt, A. Aromatic and arginine content drives multiphasic condensation of protein-RNA mixtures. *Biophysical Journal* **2023**,

(18) Mountain, G. A.; Keating, C. D. Formation of multiphase complex coacervates and partitioning of biomolecules within them. *Biomacromolecules* **2019**, *21*, 630–640.

(19) Chen, Y.; Yuan, M.; Zhang, Y.; Liu, S.; Yang, X.; Wang, K.; Liu, J. Construction

of coacervate-in-coacervate multi-compartment protocells for spatial organization of enzymatic reactions. *Chemical science* **2020**, *11*, 8617–8625.

(20) Boeynaems, S.; Holehouse, A. S.; Weinhardt, V.; Kovacs, D.; Van Lindt, J.; Larabell, C.; Van Den Bosch, L.; Das, R.; Tompa, P. S.; Pappu, R. V., et al. Spontaneous driving forces give rise to protein- RNA condensates with coexisting phases and complex material properties. *Proceedings of the National Academy of Sciences* **2019**, *116*, 7889–7898.

(21) Erkamp, N. A.; Sneideris, T.; Ausserwöger, H.; Qian, D.; Qamar, S.; Nixon-Abell, J.; St George-Hyslop, P.; Schmit, J. D.; Weitz, D. A.; Knowles, T. P. J. Spatially non-uniform condensates emerge from dynamically arrested phase separation. *Nat Commun* **2023**, *14*, 684.

(22) Alshareedah, I.; Borcherds, W.; Cohen, S.; Farag, M.; Singh, A.; Bremer, A.; Pappu, R.; Mittag, T.; Banerjee, P. Sequence-specific interactions determine viscoelastic moduli and aging dynamics of protein condensates. **2023**,

(23) Patel, A.; Lee, H. O.; Jawerth, L.; Maharana, S.; Jahnel, M.; Hein, M. Y.; Stoynov, S.; Mahamid, J.; Saha, S.; Franzmann, T. M., et al. A liquid-to-solid phase transition of the ALS protein FUS accelerated by disease mutation. *Cell* **2015**, *162*, 1066–1077.

(24) Lin, Y.; Protter, D. S.; Rosen, M. K.; Parker, R. Formation and maturation of phase-separated liquid droplets by RNA-binding proteins. *Molecular cell* **2015**, *60*, 208–219.

(25) Linsenmeier, M.; Faltova, L.; Morelli, C.; Capasso Palmiero, U.; Seiffert, C.; Küffner, A. M.; Pinotsi, D.; Zhou, J.; Mezzenga, R.; Arosio, P. The interface of condensates of the hnRNPA1 low-complexity domain promotes formation of amyloid fibrils. *Nature Chemistry* **2023**, *15*, 1340–1349.

(26) Hondele, M.; Sachdev, R.; Heinrich, S.; Wang, J.; Vallotton, P.; Fontoura, B. M.;

Weis, K. DEAD-box ATPases are global regulators of phase-separated organelles. *Nature* **2019**, *573*, 144–148.

(27) Shimanovich, U.; Michaels, T. C.; De Genst, E.; Matak-Vinkovic, D.; Dobson, C. M.; Knowles, T. P. Sequential release of proteins from structured multishell microcapsules. *Biomacromolecules* **2017**, *18*, 3052–3059.

(28) Magde, D.; Rojas, G. E.; Seybold, P. G. Solvent dependence of the fluorescence lifetimes of xanthene dyes. *Photochemistry and photobiology* **1999**, *70*, 737–744.

(29) Gutierrez, D.; Alvarez, J.; Racedo, F. Development of a steady-state fluorescence spectroscopy system and a time-resolved fluorescence spectroscopy system. Journal of Physics: Conference Series. 2019; p 012017.

(30) Lakowicz, J. R. *Principles of fluorescence spectroscopy*; Springer, 2006.

(31) Cahn, J. W.; Hilliard, J. E. Free Energy of a Nonuniform System. I. Interfacial Free Energy. *The Journal of Chemical Physics* **1958**, *28*, 258–267.

(32) Ganapathysubramanian, B.; Wodo, O. Modeling morphology evolution during solvent-based fabrication of organic solar cells. *Int. J. Mol. Sci.* **2021**, *22*, 6675.

(33) Rubinstein, M.; Colby, R. H. *Polymer Physics*; Oxford ; New York : Oxford University Press, 2007.

(34) Mugler, C. F.; Hondele, M.; Heinrich, S.; Sachdev, R.; Vallotton, P.; Koek, A. Y.; Chan, L. Y.; Weis, K. ATPase activity of the DEAD-box protein Dhh1 controls processing body formation. *Elife* **2016**, *5*, e18746.

(35) Lin, Y.-H.; Brady, J. P.; Forman-Kay, J. D.; Chan, H. S. Charge pattern matching as a 'fuzzy' mode of molecular recognition for the functional phase separations of intrinsically disordered proteins. *New J. Phys.* **2017**, *19*, 115003.

(36) Fischer, H.; Polikarpov, I.; Craievich, A. F. Average protein density is a molecular-weight-dependent function. *Protein Sci.* **2004**, *10*, 2825–2828.

(37) De Kloet, S. R.; Andrean, B. A. G. Buoyant density gradient centrifugation of RNA and DNA in alkali iodide solutions. *Biochimica et Biophysica Acta (BBA) - Nucleic Acids and Protein Synthesis* **1971**, *247*, 519–527.